Distillate flux enhancement in the air gap membrane distillation with inserting carbon-fiber spacers

Chii-Dong Ho, Luke Chen, Mei-Chih Huang, Jing-Yuan Lai & Yu-An Chen

Taylor & Francis
Taylor & Francis Group

Check for updates

Distillate flux enhancement in the air gap membrane distillation with inserting carbon-fiber spacers

Chii-Dong Ho[a], Luke Chen[b], Mei-Chih Huang[a], Jing-Yuan Lai[a], and Yu-An Chen[a]

[a]Energy and Opto-Electronic Materials Research Center, Department of Chemical and Materials Engineering, Tamkang University, Tamsui, New Taipei, Taiwan; [b]Department of Water Resources and Environmental Engineering, Tamkang University, Tamsui, New Taipei, Taiwan

ABSTRACT

A new design of air gap membrane distillation (AGMD) with inserting carbon-fiber spacers with various hydrodynamic angles in flow channels for eddy promoting under concurrent-flow operations was developed theoretically and experimentally. Attempts to enlarge eddy flow in aiming to reduce the temperature polarization were achieved with the inserted carbon-fiber spacers that enhance the heat and mass transfer in the AGMD system. A mathematical model considering heat and mass transfer mechanisms has been developed, and the Nusselt number was correlated with the experimental data. The effects of various operation parameters on the distillate flux enhancement were studied as compared to the modules without inserting carbon-fiber spacers (empty channels).

Introduction

Membrane distillation (MD) is a new alternative technology and is attracting much attention to produce drinking water by seawater desalination processes in which the production of portable water in remote villages or rural areas with the advantages of simplicity and low operating temperature make it amenable to be manufactured and for using the low-grade thermal energy in continuing developments of MD systems.[1–3] The membrane distillation of non-isothermal operations acts as a physical separation vaporizing volatile species in the hot feed fluid through porous hydrophobic membrane pores from the high to the low vapor pressure across the membrane[4,5] resulting in the high purity water production.[6]

An air gap channel is equipped in the permeate side of a membrane to allow water vapor diffusing through and in contact with the cooling plate, and the configuration is referred as the air gap membrane distillation (AGMD). The air gap membrane distillation module is best suited for pure water productivity where water vapor is the major permeate component.[7] Many investigations were focused on the modeling membrane performance,[8] and the effects of the feed flow rate and feed temperature were studied,[9,10] while comprehensive experimental and theoretical studies on the performance of an air gap membrane distillation

module were also presented to predict the pure water productivity.[7,11,12]

The temperature polarization effect building up temperature gradients in the hot saline stream leads to an decreased heat transfer[13,14] due to the heat required vaporizing water at the membrane-liquid interface, and the permeate flux is thus decreased. Reduction of the temperature polarization effect was achieved using eddy promoters in flow channel[15,16] for a favorable result to enhance the device permeate flux performance of MD operations. The purpose of the present study is to implement the carbon-fiber spacer into the improved flat plate AGMD modules and to develop a mathematical model for predicting the pure water productivity.

Mathematical modeling of the AGMD system

The mathematical modeling considering both heat and mass transfer mechanisms for AGMD systems to deepen analyzing the vapor molecules transported through porous hydrophobic membranes was investigated theoretically and experimentally. The mass transfer occurs in the porous membrane and air gap channel, while the heat transfer takes place in the domains including the hot feed, membrane, air gap, cooling plate, and cold fluid of the distillation process, as shown in Fig. 1. The
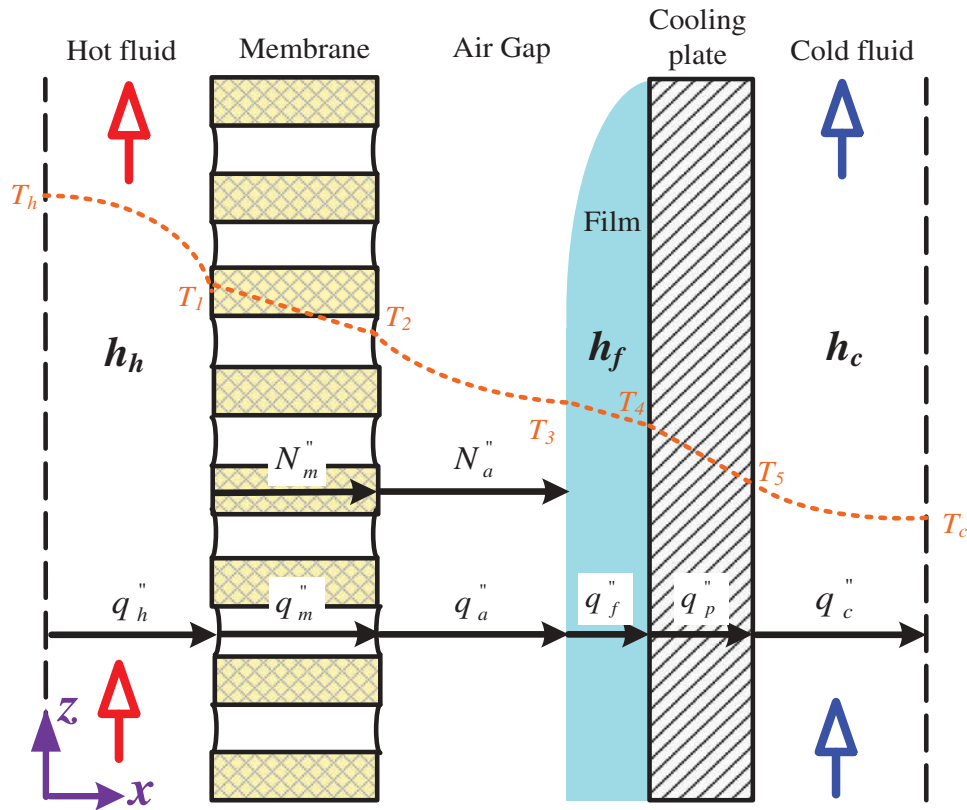
Figure 1. Heat and mass transfer mechanisms in the AGMD module.

theoretical analysis is based considering the following assumptions: (a) under steady-state operations; (b) constant physical properties of fluid, plates, and membrane; (c) stagnant air within the membrane pore; (d) the condensate forming a thin liquid film and covering the entire condensing surface; (e) mass transfer by diffusion and heat transfer by conduction within the air gap; (f) no water passing through the membrane; and (g) well insulation on the bottom and edge sides of modules.

Heat transfer

The non-isothermal process in the AGMD system creates the temperature difference across the whole module resulting in heat transfer and producing pure water. The permeate flux derived with the energy balance of enthalpy flow conservation in each heat transfer region for (1) the hot feed stream, (2) hydrophobic membrane, (3) air gap, (4) cooling plate, and (5) cooling water under the steady-state operation may be written as follows:

in the saline water region

$$q_h'' = h_h(T_h - T_1) \tag{1}$$

at the membrane

$$q_m'' = \frac{k_m}{\delta_m}(T_1 - T_2) + N''\lambda \tag{2}$$

inside the air gap

$$q_a'' = \frac{k_a}{\delta_a}(T_2 - T_3) + N''\lambda \tag{3}$$

in the permeate film with the heat transfer coefficient for the condensate film[17]

$$q_f'' = h_f(T_3 - T_4)$$
$$= 0.943\left[\frac{\rho^2 g\lambda k_f^3}{\mu L(T_3 - T_4)}\right]^{\frac{1}{4}}(T_3 - T_4) \tag{4}$$

at the condensing plate

$$q_p'' = \frac{k_p}{\delta_p}(T_4 - T_5) \tag{5}$$

in the cooling water

$$q_c'' = h_c(T_5 - T_c) \tag{6}$$

The one-dimensional modeling equation was obtained assuming well insulation on the bottom and edge sides of modules

$$q_h'' = q_m'' = q_a'' = q_f'' = q_p'' = q_c'' \tag{7}$$

The following equations can be used to describe the energy balances of hot fluid and cold fluid as

$$\frac{dT_h}{dz} = \frac{-Wq}{\dot{m}\, C_{p,h}} \tag{8}$$

$$\frac{dT_c}{dz} = \frac{Wq}{\dot{m}\, C_{p,c}} \tag{9}$$

Mass transfer

The mass transfer flux is determined considering the mass transfer resistances in series of both the membrane and air gap with neglecting the resistances in other layers. The saturation vapor pressure difference due to the temperature gradient on both membrane surfaces results in the permeate transport across the membrane accordingly, which was incorporating a membrane permeation coefficient c_m[10] to estimate the amount of permeate flux that passes through the membrane pores as

$$N_m'' = c_m \Delta P = c_m(P_1^{sat} - P_2^{sat}) \tag{10}$$

where P_1^{sat} and P_2^{sat} are the saturated pressure of water vapor calculated using the Antoine equation on the membrane surfaces in hot saline stream and the air gap, and hence, the permeate flux diffuses through the air gap and reaches to the cooling plate as the collected water condensate. For the effect of the non-volatile solute in lowering saturation vapor pressure, the water activity coefficient a_w was calculated using the correlation[5]

$$a_w = 1 - 0.5x_{NaCl} - 10x_{NaCl}^2 \tag{11}$$

$$P_1^{sat} = x_w a_w P_w^{sat} \tag{12}$$

where y_w and x_w are the vapor and water mole fractions of water, respectively, and P_w and P_1^{sat} are the total pressure and saturation vapor pressure, respectively. Moreover, the amount of the molar vapor flux diffusing through a stagnant air film over the air gap layer by molecular diffusion[18] was expressed as

$$N_a'' = c_a(P_2^{sat} - P_3^{sat}) \tag{13}$$

The overall water production was calculated by equating the permeate fluxes in the membrane and air gap, Eqs. (2) and (3), with the total mass-transfer resistances

$$N_a'' = N_m'' = N'' = c_T(P_1^{sat} - P_3^{sat}) \tag{14}$$

$$c_T = \left(\frac{1}{c_m} + \frac{1}{c_a}\right)^{-1} \tag{15}$$

Temperature polarization

Temperature polarization coefficient (TPC)[19] is an indicator to evaluate the device performance for an AGMD configuration and defined as the ratio of the temperature difference at the membrane interface to the temperature difference of the bulk temperatures:

$$TPC = \tau_{temp} = \frac{T_1 - T_3}{T_h - T_c} \tag{16}$$

The temperature polarization phenomenon in the membrane distillation systems is unavoidable and could be improved inserting the carbon-fiber spacers in flow channel as the eddy promoter in enhancing the heat transfer coefficients. The combinations of each heat flux term of Eqs. (2) and (3) and Eqs. (4)–(6) lead to the overall heat transfer coefficient of the hot stream and cooling stream, respectively

$$\begin{aligned} q''_{ma} &= q''_{cond.} + q''_{vap.} \\ &= \left\{ \left(\frac{k_m}{\delta_m} + \frac{k_a}{\delta_a}\right)^{-1} + \right. \\ &\quad \left. \left[c_T \frac{((1 - x_{NaCl})(1 - 0.5x_{NaCl} - 10x_{NaCl}^2)P_w^{sat} + P_3^{sat})\lambda^2 M_w}{2RT_{avg}^2} \right] \right\} \\ &\quad (T_1 - T_3) = H_m(T_1 - T_3) \end{aligned} \tag{17}$$

$$q''_{fc} = \frac{1}{1/h_f + \delta_p/k_p + 1/h_c}(T_3 - T_c) = H_c(T_3 - T_c) \tag{18}$$

Manipulating and solving Eqs. (17) and (18) with the aid of Eq. (1) yield

$$T_h = T_1 + \frac{H_m}{h_h}(T_1 - T_3) \tag{19a}$$

$$T_c = T_3 - \frac{H_m}{H_c}(T_1 - T_3) \tag{19b}$$

or

$$T_1 = \frac{h_h T_h + H_m T_3}{h_h + H_m} \tag{20a}$$

$$T_3 = \frac{H_c T_c + H_m T_1}{H_c + H_m} \tag{20b}$$

Substituting Eqs. (19a) and (19b) into Eq. (16) to give the temperature polarization coefficient

$$\tau_{temp} = \frac{h_h H_c}{h_h H_c + h_h H_m + H_c H_m} \tag{21}$$

Therefore, Eqs. (8) and (9) were rewritten as

$$\frac{dT_h}{dz} = \frac{-W}{\dot{m}C_{ph}} H_m \tau_{temp.}(T_h - T_c) \qquad (22)$$

$$\frac{dT_c}{dz} = \frac{W}{\dot{m}C_{pc}} H_m \tau_{temp.}(T_h - T_c) \qquad (23)$$

Experimental setup

The AGMD system and the corresponding experimental setup are illustrated in Fig. 2. The detail components of the attached carbon-fiber spacers of the AGMD module of the hot-fluid stream are illustrated in Fig. 3. The outside walls of the entire module are acrylic plates, while the carbon-fiber spacers were inserted into the hot-fluid flow channel for serving as turbulence promoters. Both the acrylic plates enclose the hot-fluid and cold-fluid channels that have three holes flowing in and out at both entrance and exit ends, respectively, to ensure evenly distributed flows. The length, width, and height of each hot and cold channel are 0.21 m, 0.29 m, and 2 mm, respectively. The hydrophobic polytetrafluoroethylene (PTFE) membrane (ADVANTEC) with a nominal pore size of 0.1 mm, a porosity of 0.72, and a thickness of 130 mm was used. The experiments were conducted for various inlet hot fluid temperatures (313, 318, 323, 328 K), inlet flow rate (0.4, 0.5, 0.7, 0.9 L/min), and inlet cold fluid temperature (298 K). Two 1 mm-thick diagonal carbon-fiber spacers with fiber width of 2 mm and 3 mm, respectively, were placed together into the hot stream side of the hydrophobic membrane with various

hydrodynamic angles, while the carbon-fiber vertical sheet was implemented as a support in the air gap channel to prevent from membrane bending and wrinkling. The permeate flux reached and condensed at the thin aluminum plate, which was collected and weighted using an electronic balance. Between the carbon-fiber sheet and aluminum plate or the acrylic plate is a 1 mm-thick silicon rubber sealing to create channels and to prevent leakage.

The numerical solution procedure

The theoretical permeate flux could be obtained by following the flow chart of calculation procedures as illustrated in Fig. 4. The temperature on both sides of membrane surfaces (T_1 and T_3), and the convective heat-transfer coefficients (h_h) were obtained iterating Eqs. (19a) and (19b) (or (20a) and (20b)) with the use of the known inlet and outlet temperatures of both hot and cold streams. The calculation procedure was displayed on the right-hand side of Fig. 4, and thus, the calculated convective heat-transfer coefficients and the temperatures of both membrane surfaces were conveyed to solve the temperatures of both hot and cold streams in Eqs. (22) and (23) by using the fourth-order Runge-Kutta method along the length of the module.

The carbon-fiber open slot spacers inserted in the conduit of hot feed stream is implemented instead of using smooth-surface channel, and the corrected factor α^E depends on the hydrodynamic angles and carbon-
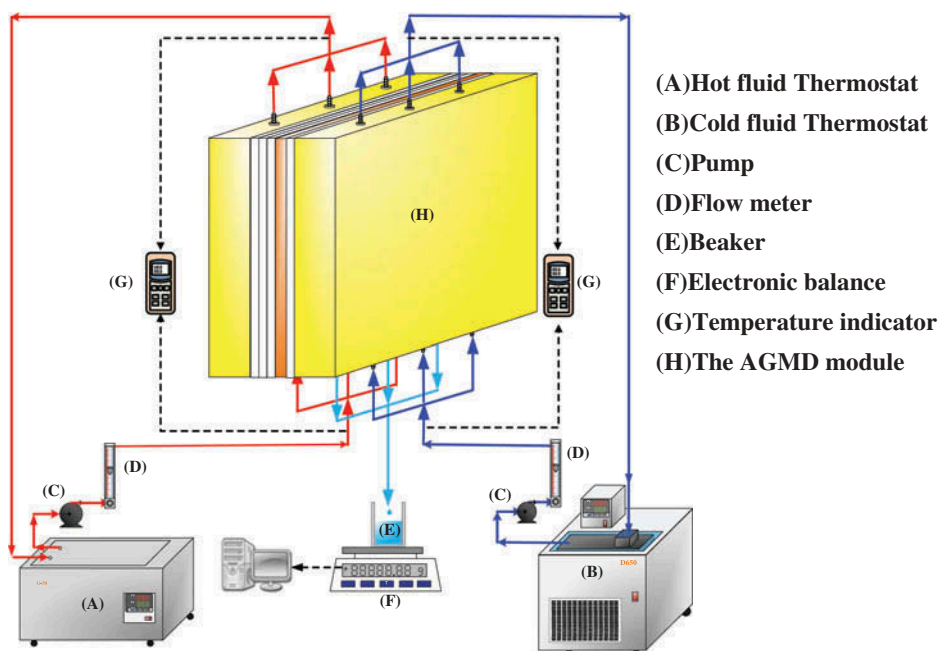
Figure 2. Experimental setup and the AGMD system.

(A) Hot fluid Thermostat
(B) Cold fluid Thermostat
(C) Pump
(D) Flow meter
(E) Beaker
(F) Electronic balance
(G) Temperature indicator
(H) The AGMD module
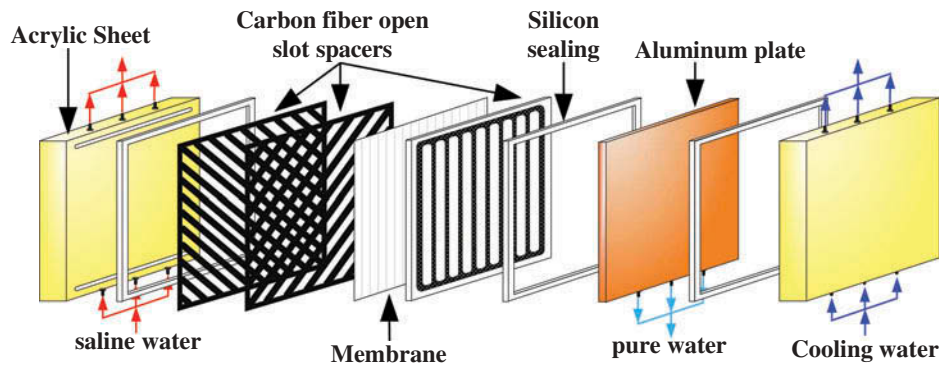
Figure 3. Components of the attached carbon-fiber spacers of the AGMD module.
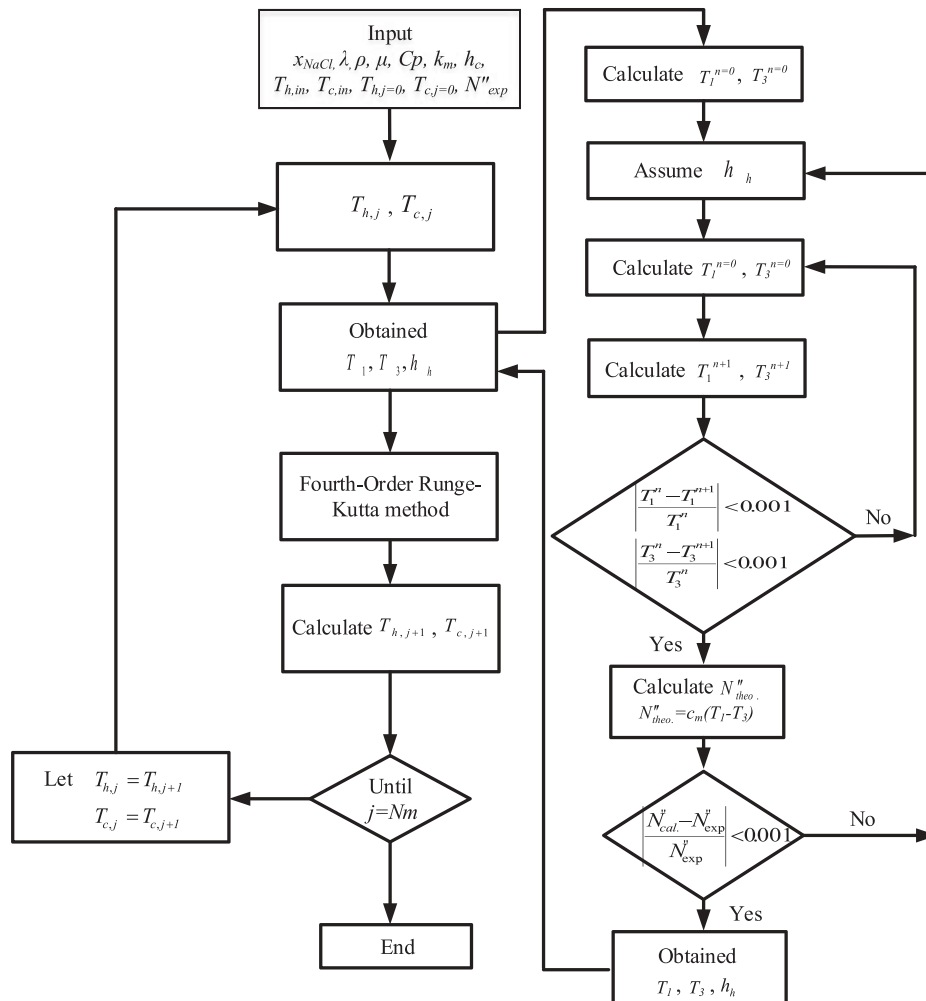
Figure 4. Calculation flow chart for solving heat transfer coefficients.

fiber widths with the characterization of the turbulent intensity as

$$Nu^E = \alpha^E Nu_{lam} \qquad (24)$$

The Buckingham's π theorem was used to obtain a simple expression of Nusselt Numbers with inserting

carbon-fiber spacers in the flow channel in terms of hydrodynamic angles and carbon-fiber widths as parameters:

$$\alpha^E = \frac{Nu^E}{Nu_{lam}} = f\left(\frac{W_e}{d_h}, \sin\theta\right) \qquad (25)$$
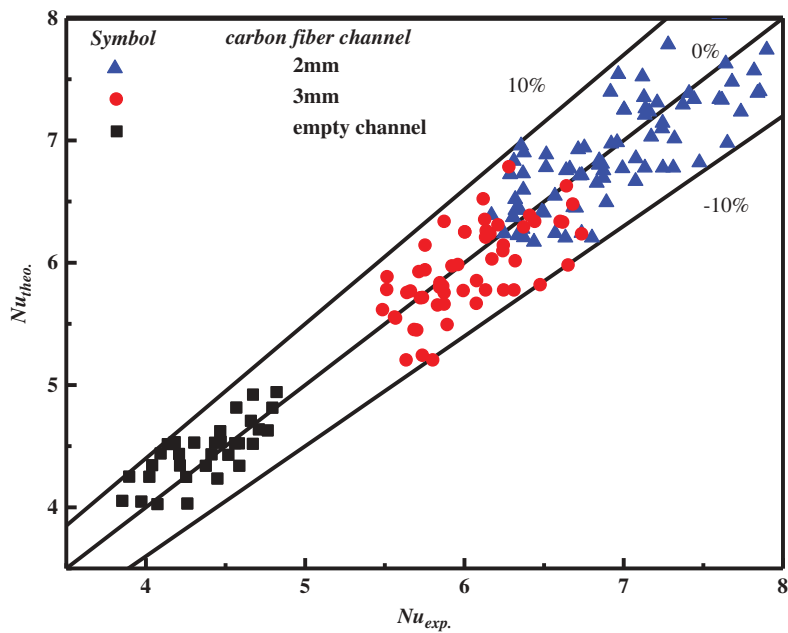
Figure 5. Comparisons of calculated and experimental Nusselt numbers.

The estimated heat-transfer coefficients h_h for inserting carbon-fiber open slot spacers in the flow channel were correlated using multiple linear regressions to obtain a simple expression of the correlation factor for heat transfer coefficient as shown in Eq. (26)

$$\alpha^E = f\left(\frac{W_e}{d_h}, \sin\theta\right) = a \exp\left(\frac{W_e}{d_h}\right)^b (\sin\theta)^c \quad (26)$$

The expression equation obtained from curve-fitting is given in Eq. (26) with the squared correlation coefficient ($R^2 = 0.97$), as shown in Fig. 5

$$Nu^E = 4.253 \exp\left(\frac{W_e}{d_h}\right)^{-0.541} \sin\theta^{-0.1321} Nu_{lam} \quad (27)$$

in which the Nusselt number of laminar flow in smooth surface channel was derived by Phattaranawik[20]
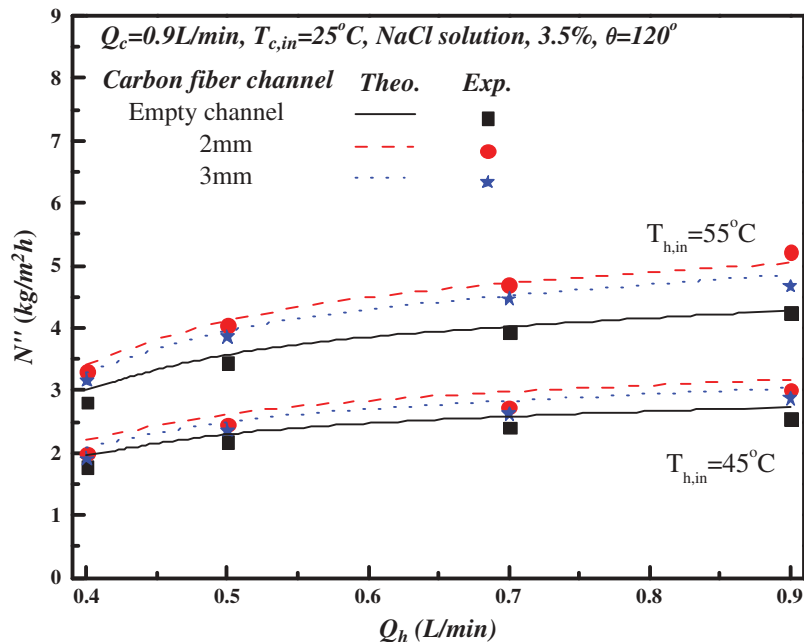
Figure 6. Effect of carbon fiber spacers on permeates flux.
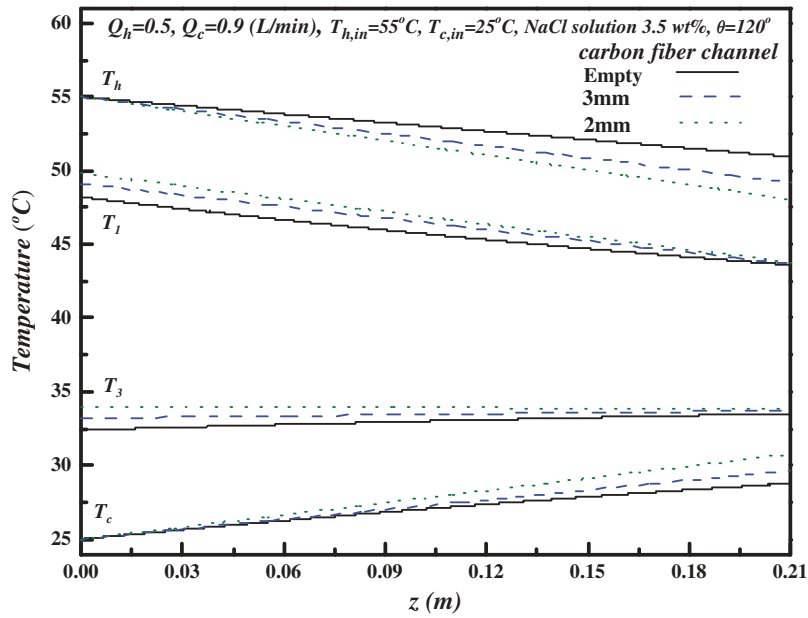
Figure 7. Effect of carbon fiber spacers on temperature distributions.

$$Nu_{lam} = 4.36 + \frac{0.036 \mathrm{Re} \Pr(d_h/L)}{1 + 0.011(\mathrm{Re} \Pr(d_h/L))^{0.8}} \quad (28)$$

The energy consumption increment is inevitable due to the increased friction in the channel when utilizing the roughened-surface. The energy consumption of an AGMD module includes both the contributions from the hot fluid side and cold fluid side and may be determined by using Fanning friction factor f_F[21]

$$P_{lost} = \dot{m}_h \ell w_{f,h} + \dot{m}_c \ell w_{f,c} = Q_h \rho_h \ell w_{f,h} + Q_c \rho_c \ell w_{f,c} \quad (29)$$

$$\ell w_{f,h} = \frac{2f_{F,h} u_h^2 L}{d_{h,h}} \quad , \quad \ell w_{f,c} = \frac{2f_{F,c} u_c^2 L}{d_{h,c}} \quad (30)$$

in which

$$d_{h,h} = \frac{4 \times \varepsilon_e}{\left(\frac{2}{d}\right) + (1 - \varepsilon_e)S_{vsp}}, \quad d_{h,c} = \frac{4DW}{2(D + W)} \quad (31)$$

The Fanning friction factor can be correlated with the aspect ratio of the channel ($\alpha = D/W$):[22]

$$f_{F,h} = \frac{C}{\mathrm{Re}_h}, \quad f_{F,c} = \frac{C}{\mathrm{Re}_c}, \quad \mathrm{Re}_h = \frac{\rho_h u_h d_{h,h}}{\mu_h}, \quad \mathrm{Re}_c = \frac{\rho_c u_c d_{h,c}}{\mu_c} \quad (32)$$

$$C = 24(1 - 1.3553\alpha + 1.9467\alpha^2 - 1.7012\alpha^3 + 0.9564\alpha^4 - 0.2537\alpha^5) \quad (33)$$

The ratio of I_N and I_P is used to evaluate the flux enhancement and energy increment, respectively, and is defined as follows:

$$I_N = \frac{N''_r - N''_s}{N''_s} \quad (34)$$

$$I_p = \frac{P_r - P_s}{P_s} \quad (35)$$

where the subscripts r and s represent the flow channels with inserting carbon-fiber open slot spacers and the smooth channel or empty channel.

Results and discussion

Both experimental results and numerical predictions of heat transfer, characterized by Nusselt number, reveal that the attached carbon-fiber spacers enhance the heat transfer of the AGMD system significantly as indicated in Fig. 5. The fairly good agreement between the experimental results and theoretical predictions for empty channel or channel with 2 mm or 3 mm carbon-fiber spacers are also demonstrated in Fig. 5. Figure 6 indicates that the permeate fluxes increase with the increasing hot inlet flow rate; however, the increment becomes insignificant at relatively higher inlet flow rate. One finds that the magnitude of the permeate flux is in the order of 2 mm > 3 mm > empty channel for all hot inlet flow rates when compared the permeate flux of the empty channel with that of the channels with inserting 2 mm and 3 mm carbon fiber spacers. The permeate flux increases with the increasing inlet hot flow rate due to the convective heat-transfer coefficient enhancement of the hot feed stream, and thus, the thinner thermal boundary layer with a lower thermal resistance results in a higher heat transfer.

Table 1. Comparisons of simulation and experimental for 2 mm carbon fiber spacers of various hydrodynamic angles on NaCl solution.

|		Saline water, NaCl = 3.5 wt%								
$T_{c,in}$ = 25°C Q_c = 0.9 L/min		Hydrodynamic angles, 2 mm								
		60°			90°			120°		
$T_{h,in}$ (°C)	Q_h (L/min)	$N''_{Exp.}$ (kg/(m² hr))	$N''_{Theo.}$ (kg/(m² hr))	error %	$N''_{Exp.}$ (kg/(m² hr))	$N''_{Theo.}$ (kg/(m² hr))	error %	$N''_{Exp.}$ (kg/(m² hr))	$N''_{Theo.}$ (kg/(m² hr))	error %
40	0.3	1.339	1.474	9.16	1.358	1.494	9.12	1.393	1.511	7.85
	0.5	1.642	1.802	8.86	1.663	1.829	9.10	1.717	1.850	7.21
	0.7	1.885	2.051	8.11	1.901	2.085	8.82	1.963	2.111	7.00
	0.9	1.962	2.115	7.22	2.012	2.155	6.63	2.033	2.191	7.18
45	0.3	1.937	2.129	9.02	1.945	2.156	9.80	1.998	2.188	8.66
	0.5	2.379	2.616	9.07	2.397	2.651	9.58	2.462	2.696	8.65
	0.7	2.623	2.884	9.04	2.660	2.927	9.10	2.730	2.975	8.23
	0.9	2.847	3.073	7.35	2.936	3.127	6.10	3.010	3.182	5.41
50	0.3	2.526	2.646	4.55	2.551	2.681	4.85	2.576	2.726	5.53
	0.5	3.051	3.342	8.71	3.141	3.394	7.46	3.220	3.455	6.79
	0.7	3.554	3.687	3.59	3.589	3.753	4.36	3.742	3.822	2.10
	0.9	3.800	3.929	3.28	3.970	4.012	1.06	4.108	4.096	0.29
55	0.3	3.016	3.319	9.11	3.119	3.366	7.34	3.308	3.420	3.28
	0.5	3.832	4.106	6.67	3.861	4.173	7.46	4.050	4.254	4.79
	0.7	4.323	4.541	4.79	4.456	4.622	3.60	4.698	4.729	0.67
	0.9	4.835	4.835	0.01	5.015	4.935	1.63	5.214	5.067	2.88
average error				6.78			6.52			5.41

Table 2. Comparisons of simulation and experimental for 3mm carbon fiber spacers of various hydrodynamic angles on NaCl solution.

		Saline water, NaCl = 3.5 wt%								
$T_{c,in}$ = 25°C Q_c = 0.9 L/min		Hydrodynamic angles, 3 mm								
		60°			90°			120°		
$T_{h,in}$ (°C)	Q_h (L/min)	$N''_{Exp.}$ (kg/(m² hr))	$N''_{Theo.}$ (kg/(m² hr))	error %	$N''_{Exp.}$ (kg/(m² hr))	$N''_{Theo.}$ (kg/(m² hr))	error %	$N''_{Exp.}$ (kg/(m² hr))	$N''_{Theo.}$ (kg/(m² hr))	error %
40	0.3	1.273	1.398	8.91	1.285	1.413	9.02	1.317	1.426	7.65
	0.5	1.562	1.716	9.02	1.579	1.737	9.11	1.626	1.754	7.32
	0.7	1.798	1.958	8.19	1.810	1.984	8.78	1.862	2.005	7.10
	0.9	1.878	2.017	6.92	1.911	2.049	6.76	1.927	2.077	7.22
45	0.3	1.863	2.040	8.72	1.872	2.061	9.20	1.908	2.087	8.57
	0.5	2.290	2.514	8.91	2.303	2.542	9.42	2.357	2.577	8.57
	0.7	2.536	2.773	8.54	2.553	2.807	9.02	2.622	2.845	7.82
	0.9	2.731	2.954	7.53	2.804	2.997	6.41	2.869	3.040	5.64
50	0.3	2.403	2.547	5.66	2.465	2.575	4.29	2.476	2.611	5.15
	0.5	2.952	3.225	8.47	3.026	3.266	7.35	3.100	3.315	6.48
	0.7	3.393	3.559	4.66	3.418	3.612	5.36	3.582	3.666	2.31
	0.9	3.649	3.791	3.73	3.810	3.857	1.21	3.907	3.923	0.42
55	0.3	2.915	3.203	9.01	3.016	3.241	6.94	3.160	3.284	3.78
	0.5	3.717	3.970	6.37	3.739	4.023	7.06	3.855	4.087	5.68
	0.7	4.215	4.390	3.98	4.311	4.455	3.23	4.471	4.541	1.53
	0.9	4.659	4.672	0.28	4.679	4.752	1.54	4.669	4.857	3.88
average error				6.81			6.54			5.57

Reduction of thermal boundary layer thickness could increase vapor pressure gradient, which results in a higher permeate flux through the hydrophobic membrane. Restated, the permeate flux increases with increasing the inlet hot fluid temperature and hot inlet flow rate. The devices with inserting carbon fiber spacers with an adequate hydrodynamic condition for eddy promoting come out with temperature polarization reduction. The permeate flux enhancement with inserting carbon fiber spacers in flow channel is clearly demonstrated in Fig. 6 for both experimental results and the theoretical predictions. The permeate fluxes were calculated through the heat transfer

coefficient correction factor, Eq. (27), for predicting the Nusselt number, as referred to the heat transfer efficiency, with inserting eddy promoter in flow channel.

The effect of the carbon fiber spacers on the temperature profiles inside the AGMD modules was shown in Fig. 7, which indicates the temperature profiles of hot fluid (T_h) are getting closer to the hot side membrane surface (T_1) when implementing the carbon fiber spacers into flow channel. The permeate flux improvement by inserting carbon fiber spacers into flow channel is confirmed from the data listed in Tables 1 and 2 with the inlet hot fluid temperature, volumetric flow
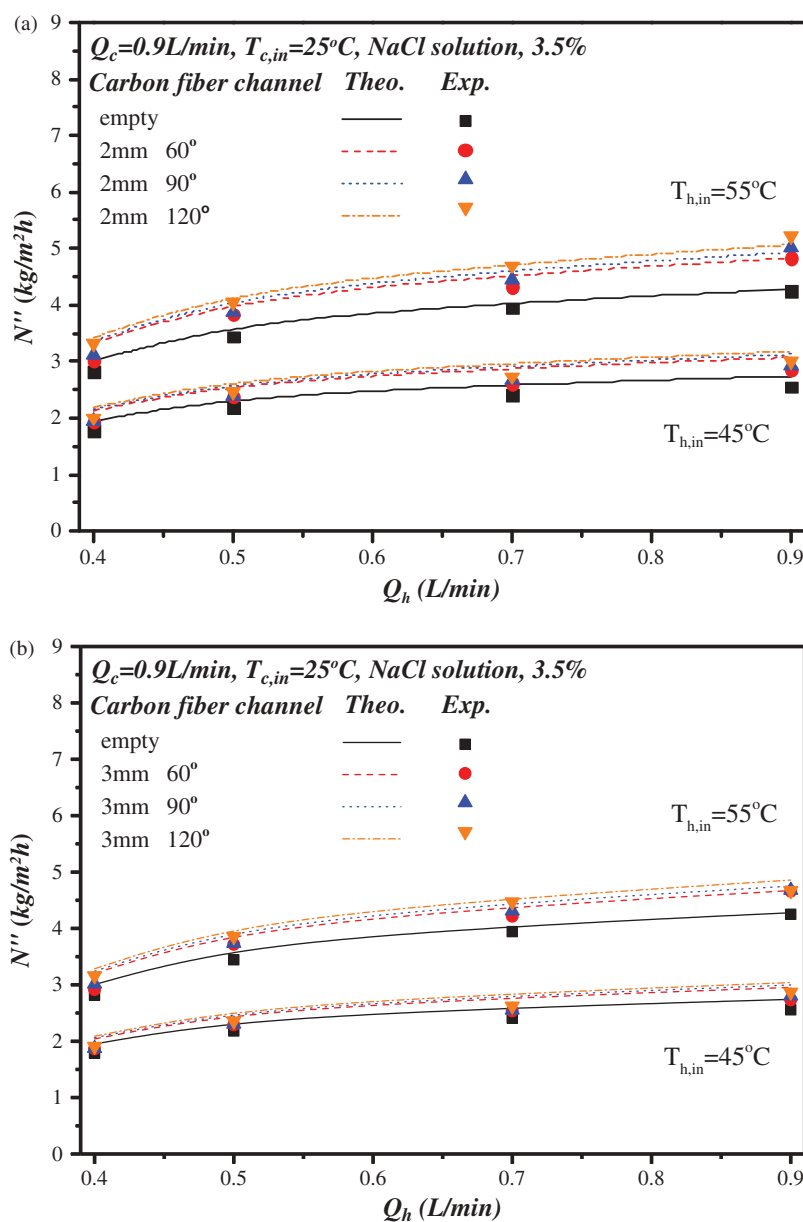
Figure 8. (a) Effect of flow channel with 2 mm carbon-fiber spacers on permeate fluxes. (b) Effect of flow channel with 3 mm carbon-fiber spacers on permeate fluxes.

rate, and hydrodynamic angle of diagonal carbon-fiber spacers as parameters. The effects of the corresponding parameters on the permeate flux were also depicted in Figs. (8a) and (8b). The effects of the operating and design parameters on the permeate flux are concluded that the higher inlet flow rate, the higher temperature, and the larger hydrodynamic angle of the carbon fiber spacer result in the higher permeate flux.

Although the permeate flux does increase with inserting carbon fiber spacers into flow channel, the increase in energy consumption due to the friction loss enlargement becomes a concern. The I_N/I_P ratio was used to evaluate the permeate flux increment per

energy consumption increment. The I_N/I_P ratio variations with inlet saline temperature, flow rate, and hydrodynamic angle of carbon fiber spacers are elucidated in Fig. 9 and Table 3. The increase of inlet saline temperature gives higher value of I_N/I_P, which reflects the expenses of energy consumption are more effective in increasing the permeate flux. In other words, the percentage of permeate flux enhancement is higher than that of energy consumption increment. The I_N/I_P ratio is also increased with increasing the volumetric flow rate, hydrodynamic angle of carbon fiber spacers. Although the Nusselt number and permeate flux of the channel with a larger width and inlet flow
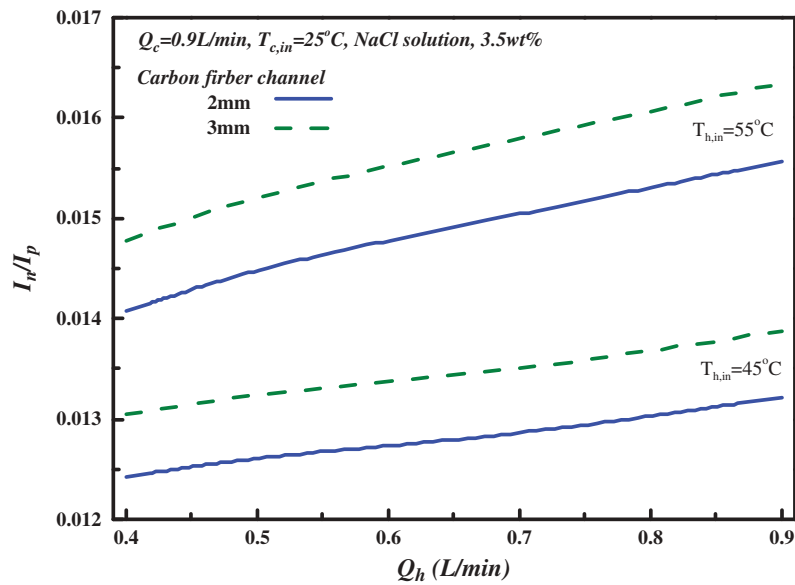
Figure 9. Effects of inlet flow rate, temperature, and carbon fiber spacer on energy efficiency of incremental permeate flux.

Table 3. Effects of operation conditions and hydrodynamic angles on the ratio of permeate flux enhancement and power consumption increment.

			Saline water, NaCl = 3.5 wt%					
			I_N/I_P					
			Hydrodynamic angles					
			60°	90°	120°	60°	90°	120°
$T_{c,in}$ (°C)	$T_{h,in}$ (°C)	Q_h (L/min)	2 mm			3 mm		
25	40	0.4	0.0088	0.0102	0.0116	0.0092	0.0108	0.0121
		0.5	0.0090	0.0105	0.0117	0.0094	0.0110	0.0122
		0.7	0.0092	0.0108	0.0120	0.0097	0.0113	0.0126
		0.9	0.0093	0.0111	0.0126	0.0098	0.0116	0.0132
	45	0.4	0.0094	0.0107	0.0124	0.0098	0.0113	0.0130
		0.5	0.0095	0.0109	0.0126	0.0100	0.0114	0.0133
		0.7	0.0098	0.0112	0.0128	0.0102	0.0118	0.0135
		0.9	0.0099	0.0116	0.0132	0.0104	0.0121	0.0139
	50	0.4	0.0098	0.0112	0.0131	0.0102	0.0118	0.0138
		0.5	0.0099	0.0115	0.0134	0.0104	0.0121	0.0141
		0.7	0.0101	0.0119	0.0137	0.0106	0.0124	0.0144
		0.9	0.0102	0.0122	0.0142	0.0108	0.0128	0.0149
	55	0.4	0.0106	0.0122	0.0141	0.0112	0.0129	0.0148
		0.5	0.0108	0.0125	0.0145	0.0113	0.0131	0.0152
		0.7	0.0109	0.0127	0.0150	0.0114	0.0133	0.0158
		0.9	0.0110	0.0130	0.0156	0.0115	0.0136	0.0163

rate are both increased, their corresponding energy consumption is also increased. However, the higher effective utilization of energy, in terms of I_N/I_P, indicates that less energy consumption increment can create much more permeate flux increment in the AGMD system.

Conclusions

The eddy promoter in flow channel of AGMD system was implemented and developed mathematically considering both the heat and mass transfer of each layer of the module and verified by experimental data. Experimental study has demonstrated its feasibility, and up to 18% of permeate flux enhancement was obtained inserting carbon fiber spacers in the flow channel of the AGMD system. The mathematical treatments in obtaining the temperature distributions and pure water productivity were presented graphically with the inlet volumetric flow rates and inlet saline temperatures as parameters. The effect of the width and hydrodynamic angle of carbon fiber spacers on the permeate flux and power consumption were delineated. Correlations of Nusselt number for

smooth channel and flow channels with inserting carbon fiber spacers have been obtained using the experimental results and theoretical predictions. These correlations indicated the flow channel using higher hydrodynamic angle gives higher permeate flux and more effective utilization of energy consumption than the one with smooth channel.

Nomenclature

a_w	Water activity in NaCl solution
c_a	Mass transfer coefficient of air gap (kg/(m^2 Pa hr))
c_m	Mass transfer coefficient of membrane (kg/(m^2 Pa hr))
c_T	Overall mass transfer coefficient (kg/(m^2 Pa hr))
C	Constant defined by Eq. (33)
$C_{p,c}$	Heat capacity of cold fluid (J/(kg K))
$C_{p,h}$	Heat capacity of hot fluid (J/(kg K))
d_h	Hydraulic diameter
D	Conduit height (m)
f_F	Fanning fraction factor
g	Gravitational acceleration (m/s^2)
h_c	Convection coefficient of cold fluid (W/(m^2 K))
h_f	Convection coefficient of condensation (W/(m^2 K))
h_h	Convection coefficient of hot fluid (W/(m^2 K))
H_c	Overall heat transfer coefficient of cold fluid (W/(m^2 K))
H_m	Thermal convection coefficient of membrane (W/(m^2 K))
I_N	Raised percentage of permeate flux (W)
I_P	Raised percentage of hydraulic loss (W)
k_a	Thermal conductivity coefficient of air gap (W/m K)
k_f	Thermal conductivity coefficient of aqueous solution (W/m K)
k_m	Average thermal conductivity coefficient of membrane (W/m K)
k_p	Average thermal conductivity coefficient of the cooling plate (W/m K)
L	Axial distance (m)
ℓw_f	Friction loss of conduits (J/kg)
$\dot{m}$	Mass flow rate (kg/s)
M_w	Molecular weight of water vapor (kg/mol)
N''	Permeate flux (kg/(m^2hr))
N_a''	Permeate flux of the air gap (kg/(m^2 hr))
N_m''	Permeate flux in the membrane (kg/(m^2 hr))
N_s''	Permeate flux for the empty channels (kg/(m^2 hr))
N_r''	Permeate flux for the carbon fiber spacer flow channel (kg/(m^2 hr))
Nu	Nusselt number
Nu^E	Nusselt number of the eddy promoter
P	Pressure (Pa)
P_1^{sat}	Saturated vapor pressure between the hot fluid and membrane surface (Pa)
P_2^{sat}	Saturated vapor pressure between the air gap and membrane surface (Pa)
P_3^{sat}	Saturated vapor pressure between the air gap and condensation surface (Pa)
P_w^{sat}	Saturated vapor pressure of pure water (Pa)
P_{lost}	Overall hydraulic loss of the hot and cold fluid (W)
P_s	Hydraulic friction loss of the empty channel (W)
P_r	Hydraulic friction loss of the carbon-fiber spacer flow channel (W)
Pr	Prandtl number
q	Heat transfer rate (W/m^2)
q_a''	Heat transfer rate between condensation and air gap membrane surface (W/m^2)
q_c''	Heat transfer rate between cooling plate and cold fluid (W/m^2)
q_f''	Heat transfer rate between condensation and cooling plate (W/m^2)
q_h''	Heat transfer rate between hot fluid and membrane surface (W/m^2)
q_m''	Heat transfer rate between membrane surface of hot fluid and air gap (W/m^2)
q_p''	Heat transfer rate of cooling plate (W/m^2)
$q_{cond.}''$	Total heat transfer rate through the membrane (W/m^2)
q_{ma}''	Total heat transfer rate of the membrane to the air gap (W/m^2)
q_{fc}''	Total heat transfer rate of the condensation to the cold fluid (W/m^2)
$q_{vao.}''$	Total heat transfer rate of water evaporation (W/m^2)
Q	Volume flow rate of fluid (m^3/s)
R	Gas constant (J/mol K)
Re	Reynolds number
S_{vsp}	specific surface of the spacer (m^{-1})
T_1	Temperature of hot fluid membrane surface (°C)
T_2	Temperature of air gap membrane surface (°C)
T_3	Temperature of condensation layer surface (°C)
T_4	Temperature of cooling plate surface at permeate side (°C)
T_5	Temperature of cooling plate surface at cold fluid side (°C)
T_c	Temperature of cold fluid (°C)
T_h	Temperature of hot fluid (°C)
T_{avg}	Average temperature of hot fluid membrane surface and condensation (°C)
u	Average fluid flow rate (m/s)
W	Conduit width (m)
W_e	Mesh width (m)
x_{NaCl}	Liquid mole fraction of NaCl
x_w	Liquid mole fraction of water
z	Conduit coordinate

Greek letters

α Conduit section rate
α^E Eddy promoter
ΔP Vapor pressure difference of membrane (Pa)
ε_e voidage of carbon-fiber spacer
λ Latent heat of water (J/kg)
μ Fluid viscosity ((N s)/m^2)
θ Angle of carbon fiber fin (degree)
ρ Density of fluid (kg/m^3)
τ_{temp} Temperature polarization coefficient
δ_a Thickness of air gap (m)
δ_m Thickness of membrane (m)
δ_p Thickness of cooling plate (m)

Subscripts

a Air gap
c Cold fluid
h Hot fluid
lam Laminar
m Membrane
$Theo.$ Theoretical
$Exp.$ Experimental

Funding

References

[1] Woo, Y.C.; Tijing, L.D.; Shim, W.G.; Choi, J.S.; Kim, S. H.; He, T.; Drioli, E.; Shon, H.K. (2016) Water desalination using graphene-enhanced electrospun nanofiber membrane via air gap membrane distillation. *Journal of Membrane Science*, 520: 99.

[2] Dehesa-Carrasco, U.; Perez-Rabago, C.A.; Arancibia-Bulnes, C.A. (2013) Experimental evaluation and modeling of internal temperatures in an air gap membrane distillation unit. *Desalination*, 326: 47.

[3] Essalhi, M.; Khayet, M. (2014) Application of a porous composite hydrophobic/hydrophilic membrane in desalination by air gap and liquid gap membrane distillation: A comparative study. *Separation and Purification Technology*, 133: 176.

[4] Alklaibi, A.M.; Lior, N. (2005) Transport analysis of air-gap membrane distillation. *Journal of Membrane Science*, 255 (1–2): 239.

[5] Lawson, K.W.; Lloyd, D.R. (1997) Membrane distillation. *Journal of Membrane Science*, 124 (1): 1.

[6] Lawson, K.W.; Lloyd, D.R. (1996) Membrane distillation. II. Direct contact MD. *Journal of Membrane Science*, 120 (1): 123.

[7] Alkhudhiri, A.; Darwish, N.; Hilal, N. (2013) Treatment of saline solutions using Air Gap Membrane Distillation: Experimental study. *Desalination*, 323: 2.

[8] Khayet, M. (2011) Membranes and theoretical modeling of membrane distillation: A review. *Advances in Colloid and Interface Science*, 164 (1–2): 56.

[9] Alsaadi, A.S.; Ghaffour, N.; Li, J.D.; Gray, S.; Francis, L.; Maab, H.; Amy, G.L. (2013) Modeling of air-gap membrane distillation process: A theoretical and experimental study. *Journal of Membrane Science*, 445: 53.

[10] Geng, H.; Wu, H.; Li, P.; He, Q. (2014) Study on a new air-gap membrane distillation module for distillation. *Desalination*, 334 (1): 29.

[11] Khalifa, A.E. (2015) Water and air gap membrane distillation for water desalination: An experimental comparative study. *Separation and Purification Technology*, 141: 276.

[12] Khalifa, A.; Lawal, D.; Antar, M.; Khayet, M. (2015) Experimental and theoretical investigation on water desalination using air gap membrane distillation. *Desalination*, 376: 94.

[13] Schofield, R.W.; Fane, A.G.; Fell, C.J.D. (1987) Heat and mass transfer in membrane distillation. *Journal of Membrane Science*, 33 (3): 299.

[14] Martínez-Díez, L.; Vázquez-González, M.I. (1998) Effects of polarization on mass transport through hydrophobic porous membranes. *Industrial & Engineering Chemistry Research*, 37: 4128.

[15] Ho, C.D.; Chang, H.; Chang, C.L.; Huang, C.H. (2013) Theoretical and experimental studies of performance enhancement with roughened surface in direct contact membrane distillation desalination. *Journal of Membrane Science*, 433: 160.

[16] Yang, X.; Yu, H.; Wang, R.; Fane, A.G. (2012) Analysis of the effect of turbulence promoters in hollow fiber membrane distillation modules by computational fluid dynamic (CFD) simulations. *Journal of Membrane Science*, 415-416: 758.

[17] Banat, F.A.; Simandl, J. (1999) Membrane distillation for dilute ethanol Separation from aqueous streams. *Journal of Membrane Science*, 163 (2): 333.

[18] Liu, G.L.; Zhu, C.; Cheung, C.S.; Leung, C.W. (1998) Theoretical and experimental studies on air gap membrane distillation. *Heat and Mass Transfer*, 34 (4): 329.

[19] García-Payo, M.C.; Izquierdo-Gil, M.A.; Fernández-Pineda, C. (2000) Air gap membrane distillation of aqueous alcohol solutions. *Journal of Membrane Science*, 169 (1): 61.

[20] Phattaranawik, J.; Jiraratananon, R.; Fane, A.G. (2003) Heat transport and membrane distillation coefficients in direct contact membrane distillation. *Journal of Membrane Science*, 212 (1–2): 177.

[21] Kandlikar, S.G.; Schmitt, D.; Carrano, A.L.; Taylor, J.B. (2005) Characterization of surface roughness effects on pressure drop in single-phase flow in minichannels. *Physics of Fluids*, 17 (10): 100606.

[22] Kakac, S.; Shah, R.K.; Aung, W. (1987) *Handbook of Single-Phase Convective Heat Transfer*, Wiley Interscience: New York.